JOURNAL OF CATALYSIS 103, 466–473 (1987)

Computer-Simulated Images of Platinum Clusters in the Channels of Y Zeolites: Zone–Axis Results

I. Y. CHAN,*,[1] R. CSENCSITS,† M. A. O'KEEFE,‡ AND R. GRONSKY‡

*Chevron Research Company, P.O. Box 1627, Richmond, California 94802-0627; and †Center for Advanced Materials and ‡National Center for Electron Microscopy, Lawrence Berkeley Laboratory, Berkeley, California 94720

Received April 27, 1986; revised October 7, 1986

Computer image simulation has been used to investigate the visibility of a 13-atom Pt cluster in the Y zeolite channel in high-resolution electron microscopy (HREM) images. This study concentrates on the effects of specimen thickness, focusing, and location of the Pt cluster. The results show that the Pt cluster is invisible if the specimen is thicker than 300 Å. Even when the specimen is thinner, the appearance of the HREM images can be very deceptive. The practical aspects of studying small particles using HREM are discussed.

INTRODUCTION

It is no longer necessary to emphasize the importance of zeolites in the field of catalysis. Although the zeolites themselves can be catalytically active, applications in commercial processes typically involve introducing catalytic metals into the zeolites. In these catalysts, the zeolites simultaneously act as supports for the metal, as molecular sieves, and as a matrix of active sites for specific chemical reactions.

There is much to be learned about the synergistic effects of the catalytic metals and their zeolite supports. Electron microscopy is an extremely valuable technique for studying these types of systems because it allows direct visualization of the microstructure, as shown in a number of publications (*1–4*), dating from 1972, which use high-resolution electron microscopy (HREM) to study the structure and defects of zeolites. The question then is, what is the smallest metal particle that can be detected by electron microscopy in such a system?

Single heavy atoms (Au, U, W, Pt) have been imaged by high-resolution electron microscopy when these atoms reside on a thin, amorphous, light-element substrate (*5, 6*). In these cases, the image formation mechanism approximates that of a weak-phase object (WPO); i.e., the images are maps of the projected potential distribution blurred by the aberrations of the objective lens. The heavy atoms appeared as dark spots while amorphous light-element support is gray in these images.

Images computed for a zeolite containing an organic molecule (*7*) have shown that the presence or absence of the molecule is indistinguishable once the thickness of the specimen becomes greater than approximately 120 Å. However, it appears plausible that a strongly scattering heavy atom or cluster should remain visible to a greater specimen thickness than the detection limit for a weakly scattering organic complex. The HREM image contrast for a periodic (crystalline) object is very complex. It possesses the symmetry of the projected structure but only resembles the structure under specific imaging conditions. Our goal is to determine the conditions under which a small (13 atoms) platinum cluster inside a Y zeolite channel can be detected by HREM. We chose the Pt/Y system because modified Y zeolites are widely used in commercial catalyst systems and Pt is a common and important catalytic metal.

0021-9517/87 $3.00

COMPUTATIONS

In this work, we concentrated on investigating how three parameters affect the visibility of the platinum cluster: specimen thickness, the platinum cluster's location within the depth of the specimen, and the objective lens defocus. All other imaging parameters were held constant.

The image simulations were carried out using the 81D version of the SHRLI (*8*) computer programs running on a VAX8600. The dynamical electron scattering calculation used the multislice (*9*) method with a slice thickness of 4.988 Å. In order to carry 3017 diffracted beams through the crystal, interactions were considered with 12097 phase-grating coefficients out to 4.22 $Å^{-1}$ in the [110] zone (out to $h,k = \pm 104$). The 4.998-Å slice containing the Pt cluster was incorporated as two "subslices" of 2.499-Å thickness each. The sum of diffracted beam intensities at 700-Å thickness was better than 0.999 for all models. The atom coordinates for the Y zeolites were taken from the work by Baur (*10*).

Images were computed for JEOL 200CX parameters: viz., spherical aberration coefficient of 1.2 mm, beam convergence semiangle of 1.0 mrad, spread-of-focus half-width of 100 Å, objective aperture corresponding to 0.5 $Å^{-1}$ and admitting 181 diffracted beams. In order to facilitate comparisons of Pt visibility among different images, all images were computed using identical gray scales.

We chose to use the objective lens characteristics corresponding to the specifications of the JEOL 200CX HREM since this is a widely used electron microscope. The maximum specimen thickness assumed was 700 Å because that is the maximum thickness of a good microtomed thin section. The zeolite crystal was oriented with the electron beam down the [110] zone axis, parallel to the zeolite channels. The Pt cluster consists of one atom surrounded by six atoms in a plane with three atoms above and three atoms below; i.e., it retains the threefold symmetry of the Pt(111) planes. Simulations with the Pt cluster in random orientations showed identical results as to its visibility.

RESULTS

Figure 1 shows the projected potential map of the Y zeolite unit cell in [110] projection and how the 13-atom Pt cluster was assumed to fit in the channel. This is how the image would look using a microscope with infinite resolution and no diffraction effects.

Figure 2 shows weak-phase object images of Y zeolite in [110] projection with no Pt cluster. A WPO image is merely a projection of the crystal potential in the electron beam direction, calculated at a selected resolution. A WPO image is thus a microscope-independent, idealized image; i.e., it is the image that the electron microscope is assumed to produce from a thin specimen viewed at optimum defocus. Of

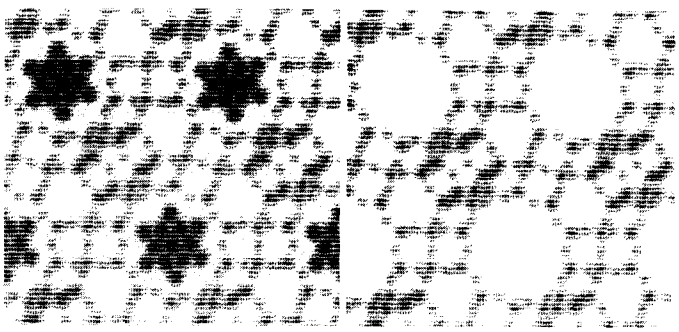

FIG. 1. Projected [110] potential map of the Y zeolite unit cell with (left) and without (right) the 13-atom Pt cluster in the channel.

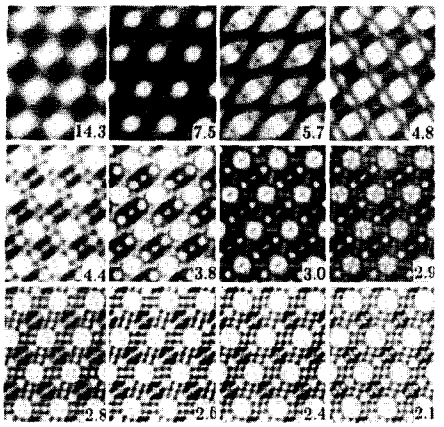

FIG. 2. Computed weak-phase object (projected potential) images of Y zeolite in [110] projection; resolutions are marked.

course, how well an actual image corresponds to the WPO image depends on both the specimen and the electron microscope. Figure 2 shows WPO images of Y zeolite in [110] projection for a range of resolutions from 14 to 2 Å and demonstrates how the structure should appear at each resolution under optimum conditions. Note that the empty tunnel appears to be occupied by a dark patch for image resolutions between 3.77 and 2.8 Å. This is due to the loss of the higher frequencies needed to accurately describe the almost square-well potential of the channels. When sufficient higher frequencies are included by increasing the resolution to 2.6 Å or better, the tunnels appear clear.

The WPO images in Fig. 2 were produced by assuming that two approximations hold: (1) that the specimen is thin enough for a kinematic (single-scattering) description of the electron scattering to produce a close approximation to the specimen exit-surface electron wave, and (2) that the objective lens could be adjusted to a condition under which it imposes a $\pi/2$ phase change on all spatial frequencies up to the values of resolution that are marked in the figure.

All WPO images are idealized projections of the specimen potential (to a limited resolution), whereas images simulated by using the full dynamical-scattering (multislice) theory include the effects of both amplitude and (strong) phase scattering. Followed by a proper application of wave-optics theory, including lens aberrations, multislice calculations produce simulated images that match real images and thus demonstrate how real images can be expected to deviate from the WPO ideal due to imaging conditions departing from the ideal WPO conditions.

The set of simulated electron microscope images that we computed is depicted by the matrix shown in Table 1. There are five sets of Y zeolite images: without any Pt cluster [$I(1)$ to $I(8)$], with the Pt cluster at the center of the 1st unit cell [$I(9)$ to $I(16)$], with the Pt cluster at the 9th unit cell [$I(17)$ to $I(19)$], with the Pt cluster at the 14th unit cell [$I(20)$ and $I(21)$], and with the Pt cluster at the

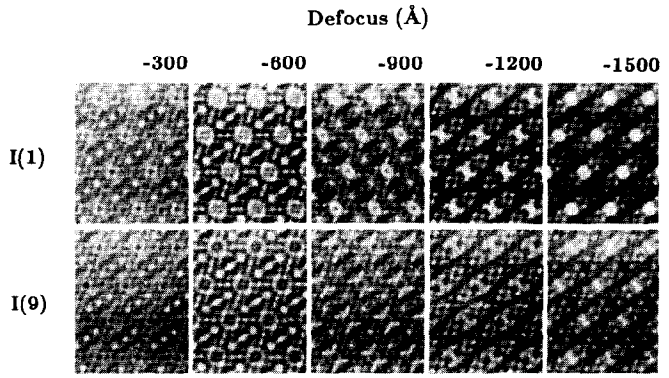

FIG. 3. Simulated Y zeolite images. Specimen thickness = 35 Å. $I(1)$ without Pt; $I(9)$ with Pt. Bar = 14.3 Å.

TABLE 1

Computation Matrix

Specimen thickness (Å)	Unit cell	Number of slices	Placement of Pt atom cluster				
			0	Pt_1	Pt_2	Pt_3	Pt_4
35	1	7	*I*(1)	**I*(9)			
70	2	14	*I*(2)	*I*(10)			
105	3	21	*I*(3)	*I*(11)			
140	4	28	*I*(4)	*I*(12)			
175	5	35	*I*(5)	*I*(13)			
315	9	63	*I*(6)	*I*(14)	**I*(17)		
500	14	98	*I*(7)	*I*(15)	*I*(18)	**I*(20)	
700	20	140	*I*(8)	*I*(16)	*I*(19)	*I*(21)	**I*(22)

Note. *Indicates the location of Pt cluster.

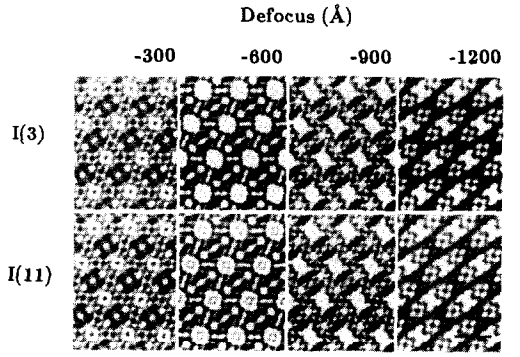

FIG. 5. Simulated Y zeolite images. Specimen thickness = 105 Å. *I*(3) without Pt; *I*(11) with Pt. Bar = 14.3 Å.

20th cell [*I*(22)]. Within each set, the images are computed for different specimen thicknesses. For example, *I*(11) is the image of a 105-Å-thick specimen with a Pt cluster located within the 1st unit cell, and *I*(18) is the image with the Pt cluster located within the 9th unit cell of a 500-Å-thick specimen.

In each case, images are calculated for five focus settings: $\Delta f = -300$, -600, -900, -1200, and -1500 Å. Except for the 35-Å thickness, all the images of the same specimen thickness at -1200 and -1500 Å underfocus do not show any differences between those with Pt and those without. In fact, for thicknesses above 300 Å, all the images of the same defocus and the same thickness are identical regardless of the presence and the location of the Pt cluster.

Figures 3 through 9 display the images produced by the computations. The presence of the Pt cluster is detected in every focus setting in the 35-Å-thick specimen (Fig. 3). However, the Pt is detected only by comparing the images. The images of the pure Y zeolite (no Pt) show dark patches in the zeolite channels at -300, -600, and -900 Å focus settings. The dark patches arise from missing spatial frequencies produced by the strongly scattering zeolite matrix.

At 70 Å thick, the images are the same both with and without Pt for -300 and -1200 Å defocus (Fig. 4). The presence of Pt creates darker contrast inside the channel when $\Delta f = -600$ and -900 Å. The same is true for the 105- and 140-Å-thick specimens (Figs. 5 and 6) except that the contrast of the Pt images inside the channels decreases with increasing thickness. In

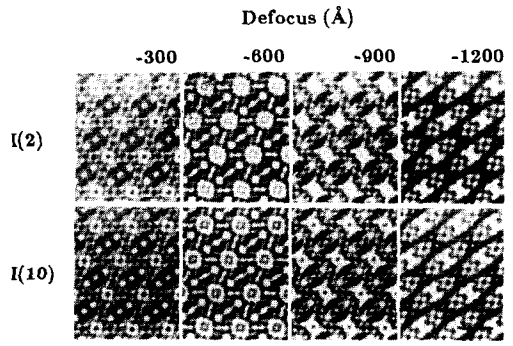

FIG. 4. Simulated Y zeolite images. Specimen thickness = 70 Å. *I*(2) without Pt; *I*(10) with Pt. Bar = 14.3 Å.

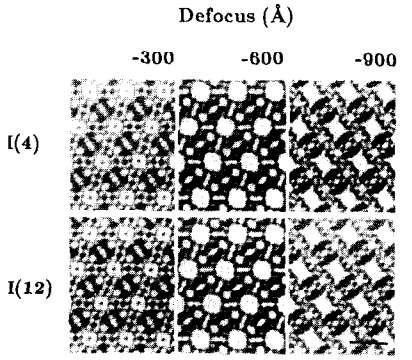

FIG. 6. Simulated Y zeolite images. Specimen thickness = 140 Å. *I*(14) without Pt; *I*(12) with Pt. Bar = 14.3 Å.

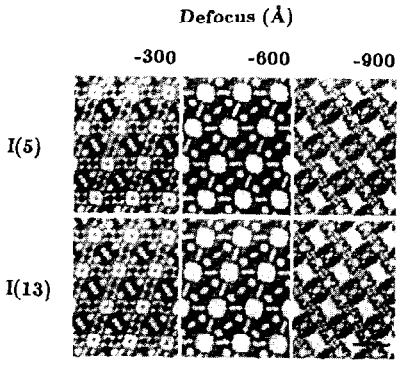

FIG. 7. Simulated Y zeolite images. Specimen thickness = 175 Å. $I(5)$ without Pt; $I(13)$ with Pt. Bar = 14.3 Å.

fact, the Pt image completely disappears at $t = 140$ Å, $\Delta f = -900$ Å. On the other hand, the zeolite images remain unchanged for the same focus settings as thickness increases. The same applies to the images of the 175-Å-thick specimen (Fig. 7), except that the Pt image at −600 Å defocus is very faint.

Figure 8 shows that at the 315-Å thickness the zeolite has the same contrast whether the Pt cluster is situated near the top or bottom of the specimen, or indeed whether it is absent altogether. Figure 9 shows the computed images of Y zeolites without Pt at 500- and 700-Å specimen thickness. All the other images of the same thickness are the same whether or not they contain the Pt cluster. They are also independent of the location of the Pt cluster in the channel. In other words, the Pt cluster is invisible for specimens thicker than 300 Å.

In all the images calculated near optimum defocus (*11*) (−600 Å for the JEOL 200CX), dark patches appear at the tunnel positions even when no Pt is present; this effect occurs even for thin crystals (Fig. 3). Such thin-crystal, optimum-defocus images should appear very similar to a WPO image of the same resolution; however, the −600 Å defocus image (Fig. 3), while otherwise very similar to the 2.4-Å WPO image (Fig. 1), includes the dark patch at the tunnel position. The explanation for this "anomalous" dark contrast is provided by the contrast-transfer function (CTF) of the 200CX electron microscope. Figure 10 shows how the lowest frequency reflection from Y zeolite ((111) in the [110] orientation) is largely blocked by phase shifts in the objective lens of the 200CX at −600 Å defocus; only approximately 21% of its amplitude is passed to contribute to the image, and it is the missing (111) frequency that produces the dark patch. Figure 11 shows the effect on the WPO image of blocking this 14-Å frequency entirely; the dark patch, previously only present in those full WPO images with resolutions between 3.77 and 2.86 Å, now extends from 4.76 Å all the way to 1.5 Å. It is this dark patch which makes it so difficult to detect the presence of Pt in Y zeolite.

Figure 12 shows how the blocking of additional low-frequency terms produces even more of a dark patch at the tunnel position in annular weak-phase object (AWPO) images. This effect means that as electron microscopes resolution is improved the problem of Pt cluster visibility at Scherzer defocus in large unit cell zeolites will worsen, rather than get better. This effect may be obviated to some degree by using larger values of underfocus (con-

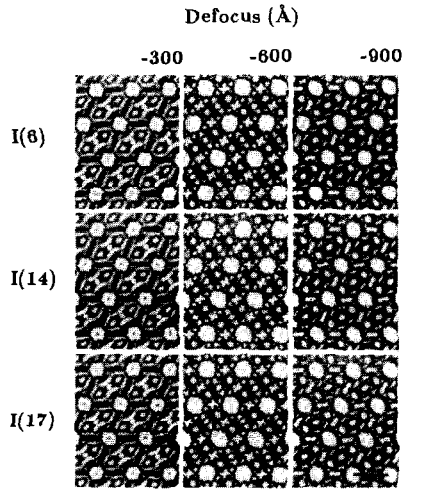

FIG. 8. Simulated Y zeolite images. Specimen thickness = 315 Å. $I(6)$ without Pt; $I(14)$ with Pt in 1st unit cell; $I(17)$ with Pt in 9th unit cell. Bar = 14.3 Å.

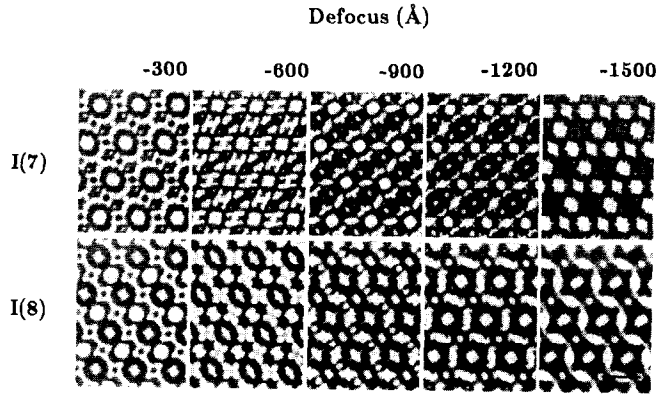

FIG. 9. Simulated images of zeolites without the Pt cluster. $I(7)$ at 500 Å thickness; $I(8)$ at 700 Å. Bar = 14.3 Å.

sider the differences visible at Scherzer focus (−600 Å) in Fig. 3, compared with the differences at larger values of defocus such as −900 through −1500 Å).

DISCUSSION

The calculations show that unambiguous images of the 13-atom Pt cluster residing in the channel of a zeolite can be obtained only under very specific conditions. Furthermore, these conditions are not likely to be met under the normal experimental conditions. The results reinforce the fact that electron microscopy images should not be interpreted intuitively, especially when near the resolution limit of the instrument.

We must now put the applications of HREM to heterogeneous catalysts in perspective in light of these results. Part of the reason that the 13-atom cluster is difficult to

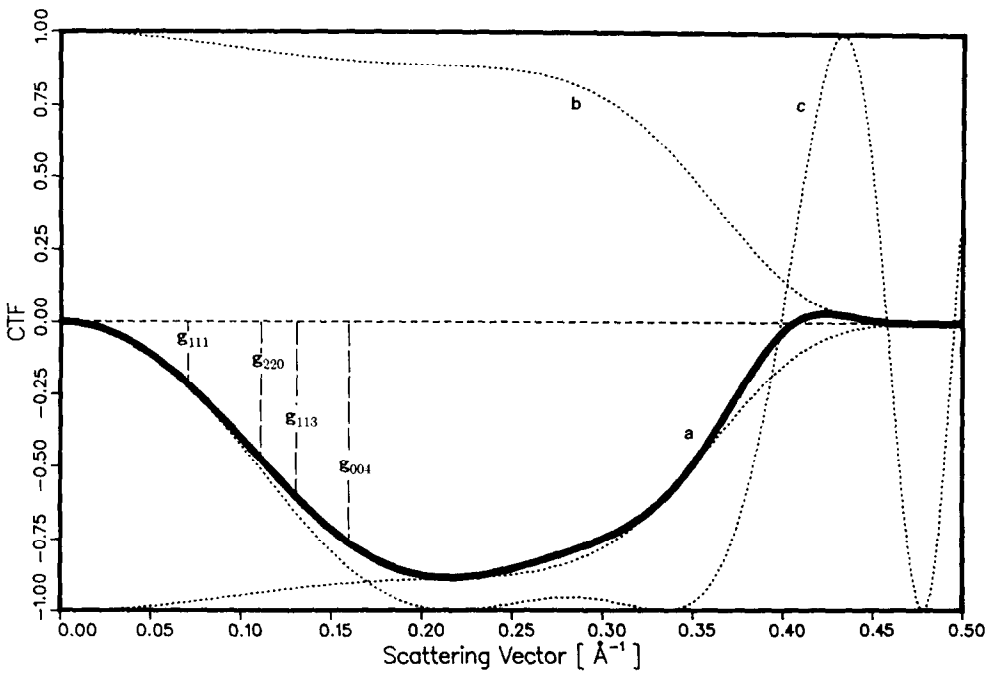

FIG. 10. Contrast transfer function. Damped CTF for the 200CX (a), formed by imposing the envelope function (b), on the undamped CTF (c). Y zeolite spacings are marked for the four lowest spatial frequencies.

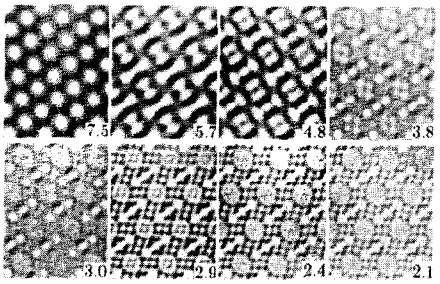

FIG. 11. Annular weak-phase object images of Y zeolites with frequencies below 0.1 Å^{-1} (spacings greater than 10 Å), blocked, computed for resolutions marked.

FIG. 12. Annular weak-phase object images of 2.4-Å resolution, but with values for blocking of low frequencies increasing from 0 to 0.16 Å^{-1}. The lowest frequency present in each AWPO image is marked. Note that 0.07, 0.11, 0.13, and 0.16 Å^{-1} correspond to resolutions of 14.3, 8.7, 7.5, and 6.2 Å, respectively.

detect in the calculated images is that the contribution of the periodicity of the matrix to the image contrast is very strong. This "overwhelms" the contrast of the Pt cluster. When the zeolite is not oriented exactly along a major zone axis, the matrix contribution to the contrast would be substantially smaller, rendering the Pt cluster more visible. During the observation, the zeolite often loses its crystallinity with time. This should also increase the visibility of small metal particles. Image simulation studies of these imaging conditions will be the subject of future communications.

Another aspect of studying small particles is the question of detectability. For example, a 5-Å metal particle might not appear as a well-defined 5-Å spot in the image; nonetheless it can be detected as a recognizably different (from the surrounding) image feature, although it undoubtedly will be a rather fuzzy image. There are many techniques in electron microscopy devised to enhance this detectability, such as hollow-cone TEM imaging; digital image processing; and combined electron energy loss and STEM annular dark field imaging.

It should be pointed out that the image simulations presented here are for a 13-atom cluster which is theoretically about 8.3 Å across. Yet, not all 8-Å particles consist of exactly 13 atoms. In fact, the number of atoms in a particle increases almost to the third power of its lateral dimension; e.g., a 20-Å particle contains ~450 atoms, and a 50-Å particle contains ~7000 atoms.

Lastly, there is one factor that acts in the experimenter's favor if detecting the presence of small particles is the main objective. The computed images show that the zeolite images are essentially the same for thickness differences less then 80 Å. For nonparallel-sided specimens with taper angles of less than 20°, this means that zeolite channels separated by less than 200 Å should possess about the same contrast. Thus if there is a significant image contrast difference between neighboring channels, it should be a good indication that a small Pt cluster is present in the channel that looks different from the others. Of course, this is true only when the distribution of Pt is not the same for every zeolite channel.

CONCLUSIONS

The computed images show that the 13-atom Pt cluster cannot be imaged in the [110] orientation using the 200CX HREM if the specimen is thicker than 300 Å. Even when the specimen is thin, correct interpretation of the image contrasts can be very tricky. Intuitive interpretation definitely does not work! However, there are many experimental factors that favor the detection of small Pt clusters. The odds improve very quickly with increasing particle size.

ACKNOWLEDGMENTS

We thank R. Kilaas for supplying the curve in Fig. 10. R. Csencsits, M. A. O'Keefe, and R. Gronsky acknowledge support from the Director, Office of Energy Research, Office of Basic Energy Sciences, Materials Sciences Division, U.S. Department of Energy, under Contract DE-AC03-76SF00098.

REFERENCES

1. Frety, R., Ballivet, D., Barthomeuf, D., and Trambouze, Y., *C.R. Acad. Sci. Paris* **275,** 1215 (1972).
2. O'Keefe, M. A., Sanders, J. V., and Mainwaring, D., *in* "Eighth International Congress on Electron Microscopy," Vol. 1, p. 518, 1974.
3. Thomas, J. M., and Millward, G. R., *J. Chem. Soc. Chem. Commun.*, p. 1380 (1982).
4. Terasaki, O., Thomas, J. M., and Millward, G. R., *Proc. R. Soc. A* **395,** 153 (1984).
5. Formanek, H., Muller, M., Hahn, M., and Koller, T., *Naturwissenschaften* **58,** 339 (1971).
6. Iijima, S., *Optik* **48,** 193 (1977).
7. Rai, R. S., O'Keefe, M. A., and Thomas, G., *in* "Proceedings of the 43rd Annual Meeting of EMSA, 1985" (G. W. Bailey, Ed.), p. 372, San Francisco Press, San Francisco.
8. O'Keefe, M. A., and Buseck, P. R., *Trans. Amer. Crystallogr. Assoc.* **15,** 27 (1979).
9. Goodman, P., and Moodie, A. F., *Acta Cryst. A* **30,** 280 (1974).
10. Baur, W. H., *Amer. Mineral.* **49,** 698 (1964).
11. Scherzer, O., *J. Appl. Phys.* **20,** 20 (1949).